# THERMODYNAMICS OF MOVING AND MELTING ICE SLURRIES

**O. SARI, F. MEILI, D. VUARNOZ**
University of Applied Sciences of Western Switzerland
CH-1401 Yverdons-les-Bains, Switzerland

**P. W. EGOLF**
Swiss Federal Laboratories for Materials Testing and Research
CH-8600 Dübendorf, Switzerland

The heat transport to a talin/water ice slurry in a cylindrical heat exchanger was determined by theory and experiment. The theory based on perturbation analysis is only valid for small heat transfer rates. Dirichlet and Neumann boundary conditions are applied to numerically calculate temperature profiles at different distances downstream. For the constant-heat-flux-density boundary condition (Neumann b. c.) numerical results are compared with measured profiles. Of laminar and low-Reynolds-number turbulent flows heat transfer coefficients are presented as a function of the Hedström number.

## INTRODUCTION

The basic thermodynamic theory of a Newtonian fluid flowing through a tube goes back to the studies of Graetz in 1885 [1]. He realized that the differential equation can be separated to obtain exponential functions to describe the behaviour downstream and that the velocity profile in the radial direction can be described by a series of Bessel functions. In 1956 Grigull wrote a treatise on heat transfer of Non-Newtonian fluids [2]. His work deals with the description of the behaviour of pseudo-plastic fluids and Bingham fluids. In 1959 Wissler and Schechter extended the Graetz-Nusselt problem to Bingham fluids [3]. One year later Thomas [4] studied the thermodynamics of a flowing Bingham of aqueous thorium oxide suspensions for applications in nuclear reactors. To our best knowledge this work comes closest to the thermodynamic problem of a moving and melting ice slurry flow, and therefore some results of the nuclear physics work can be applied. An important difference is that for the atomic material there is a necessity to introduce a source term, describing the energy production by the nuclear reaction in the bulk of the fluid. Such a source term does not occur in ice slurry flows. On the other hand the behaviour of an ice slurry can only be described by additionally taking a melting model into consideration (see Ref. [5]).

## 1. BASIC THEORY

In Ref. [6] the basic system of equations, which can be derived from the continuity, the Navier Stokes and the energy equation are presented

$$\frac{\partial \rho}{\partial T}\frac{\partial T}{\partial x}u + \rho\frac{\partial u}{\partial x} = 0\,. \tag{1}$$

$$\rho u\frac{\partial u}{\partial x} + \frac{\partial p}{\partial x} - \frac{\mu}{r}\frac{\partial u}{\partial r} - \frac{1}{r}\tau_0 - \frac{\partial \tau_0}{\partial T}\frac{\partial T}{\partial r} - \frac{d\mu}{dT}\left(\frac{\partial u}{\partial r}\frac{\partial T}{\partial r}\right) - \mu\frac{\partial^2 u}{\partial r^2} = 0\,. \tag{2}$$

$$\rho u c_p\frac{\partial T}{\partial x} - \frac{k}{r}\frac{\partial T}{\partial r} - \frac{dk}{dT}\left(\frac{\partial T}{\partial r}\frac{\partial T}{\partial r}\right) - k\frac{\partial^2 T}{\partial r^2} = 0\,. \tag{3}$$

## 2. PERTURBATION ANALYSIS

In this article only small thermal forcings of the system are considered. Then a perturbation analysis - to linearize the system of equations – is applied. All the physical properties are split into a basic function and a perturbation quantity

$$\chi = \chi^{(0)} + \chi^{(1)}, \qquad \chi \in \{u, p, T\}. \tag{4}$$

Now, we demand that

$$\left|\chi^{(1)}\right| << \left|\chi^{(0)}\right|. \tag{5}$$

The zero-order quantities of the physical properties are taken to be constant and equal to those at the inlet of the heat transfer tube, with a constant temperature across the inlet section. Furthermore, the zero-order solution is assumed to be identical to the isothermal solution, which describes a plug flow. Therefore, it follows that

$$\frac{\partial}{\partial \sigma}\chi^{(0)} = 0, \qquad \chi \in \{\rho, T\}, \qquad \sigma \in \{x, r\}, \tag{6}$$

with the isothermal solution being (see Ref. [7])

$$u^{(0)} = \left\{ \begin{array}{ll} -\dfrac{1}{4\mu}\dfrac{\partial p}{\partial x}(r_2 - r_1)^2, & 0 \le r \le r_1 \\ -\dfrac{1}{4\mu}\dfrac{\partial p}{\partial x}\left[\left({r_2}^2 - r^2\right) - 2r_1(r_2 - r)\right], & r_1 \le r \le r_2 \end{array} \right\}, \tag{7a,b}$$

where $r_1$ defines the plug radius and $r_2$ the pipe radius. Substituting (4) into (1) and applying (5) and (6) it follows that

$$\frac{\partial u^{(1)}}{\partial x} = 0\,. \tag{8}$$

This is a very important result. The perturbation of the velocity does not change downstream. And because there is no perturbation at the inlet, it can be concluded that the velocity profile does not alter at all. If a small heating rate is applied, the isothermal velocity profile is very stable. There must be a high forcing of the system to activate the coupling between the velocity and the temperature field. One concludes that only high heating rates can distort the isothermal velocity profile.

The same procedure is applied to the Navier Stokes equation. The final result is

$$\frac{\partial^2 u^{(1)}}{\partial r^2}+\frac{1}{r}\frac{\partial u^{(1)}}{\partial r}+\frac{1}{\mu^{(0)}}\left\{\left.\frac{d\tau_0}{dT}\right|_{T_0}\frac{\partial T^{(1)}}{\partial r}+\left[\left.\frac{d\mu}{dT}\right|_{T_0}\left(\frac{\partial u^{(0)}}{\partial r^2}+\frac{1}{r}\frac{\partial u^{(0)}}{\partial r}\right)+\frac{1}{r}\left.\frac{d\tau_0}{dT}\right|_{T_0}\right]T^{(1)}-\frac{\partial p^{(1)}}{\partial x}\right\}=0 \tag{9}$$

By a perturbation analysis the energy equation is transformed to a diffusion-type partial differential equation, describing convective transport

$$\frac{\partial T^{(1)}}{\partial x}-\frac{a^{(0)}}{u^{(0)}}\left(\frac{1}{r}\frac{\partial T^{(1)}}{\partial r}+\frac{\partial^2 T^{(1)}}{\partial r^2}\right)=0\,. \tag{10}$$

The energy equation – describing the behaviour of a slightly forced steady state flow in a tube – is identical for a non-melting and a melting Bingham fluid (compare with results in Ref. [8]).

Inserting the isothermal solution into equation (9) leads to

$$\frac{\partial p^{(1)}}{\partial x}=\left.\frac{d\tau_0}{dT}\right|_{T_0}\left(\frac{\partial T^{(1)}}{\partial r}+\frac{1}{r}T^{(1)}\right), \qquad 0\le r\le r_1$$

$$\frac{\partial p^{(1)}}{\partial x}=\left.\frac{d\tau_0}{dT}\right|_{T_0}\frac{\partial T^{(1)}}{\partial r}+\left[\frac{1}{2\mu^{(0)}}\left.\frac{d\mu}{dT}\right|_{T_0}\frac{\partial p^{(0)}}{\partial x}\left(2-\frac{r_1}{r}\right)+\frac{1}{r}\left.\frac{d\tau_0}{dT}\right|_{T_0}\right]T^{(1)}, \qquad r_1\le r\le r_2. \tag{11a,b}$$

The equations (8), (10) and (11) - together with the solution for the zero-order velocity (7) and appropriate boundary conditions at the inlet and on the tube wall - define the problem for small heat transfer rates. The momentum transfer equation (11) has been transformed to a condition, which gives a linear correction to the pressure drop. Because of the heat input the ice slurry melts and with the temperature also the viscosity and the critical shear stress decrease. Caused by this the pressure decreases less than in an isothermal flow with an identical inlet temperature. All the terms on the right hand side of equation (11) are positive. This reduces the absolute value of the negative directional pressure derivative.

To obtain temperature profiles according to equation (10) a usual discretization scheme had been applied and the problem was programmed in Delphi 4. Numerically calculated temperature profiles are shown in chapters 5 and 6.

## 3. TEST FACILITY "COULIS"

The refrigeration device has a refrigeration power of 9 kW and is connected to an Integral ice generator (see figure 1). Main parts of the device are also described in Ref. [9]. The secondary fluid is a water/talin mixture with 10 mass % talin. Analogous conditions as in FIFELAB, at the University of Applied Sciences of Central Switzerland (UASCS), have been chosen. Even the design of the storage tanks and the used mixing elements are of the same type. This is advantegeous, because it gives the possibility to make comparisons in introductory testing experiments and to standardize the equipments. In figure 1 the visualization device is shown used by Sari et al. to produce microscopic

pictures and to measure flow profiles (see Ref. [10]). Of higher importance for the presented work in this article is the cylindrical heat exchanger shown on the right hand side of figure 1. A more detailed drawing of it is presented in figure 2.

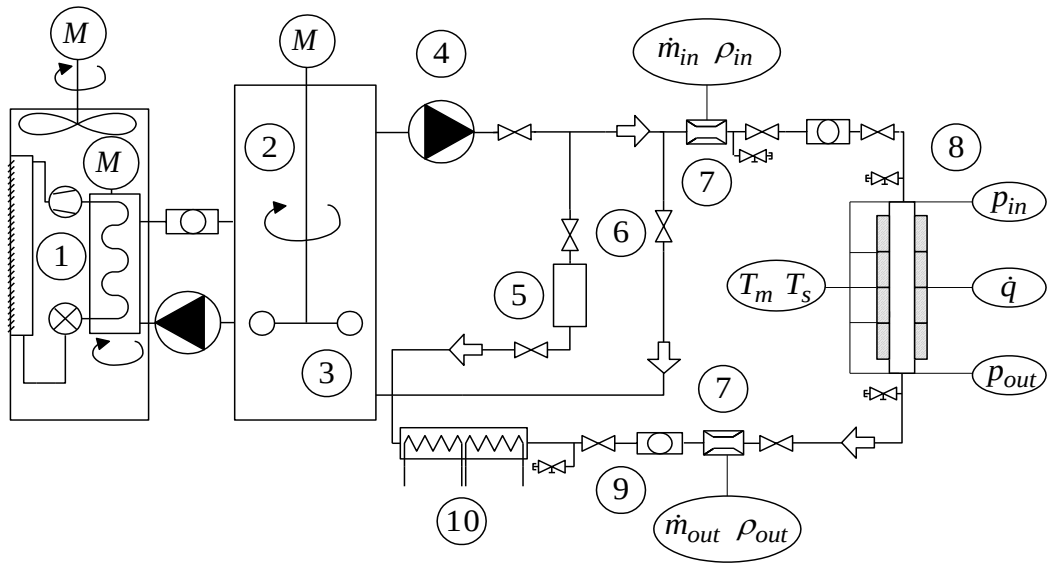


| | |
|---|---|
| 1 | Refrigerating machine and ice generator: Unelco 2.5 TR |
| 2 | Storage tank: 1000 liter |
| 3 | Mixing element: Visco Jet |
| 4 | Pump: Grundfos CRE/CRNE , 6 stages, motor: 0.75 kW, 0 – 1 kg/s |
| 5 | Microscopic visualization of ice particles |
| 6 | Bypass |
| 7 | Mass flow meter: Endress & Hauser Promass 63F |
| 8 | Heat exchanger |
| 9 | UVP measurement |
| 10 | Electric heaters: Mösch, 9kW |

Valve
Drain-valve
Flow
Compressor
Pressure reducer
Pump
Flow meter
Sight glass
M Motor

Figure 1: The experimental device “COULIS” with a refrigeration machine and an ice generator with mechanically rotating scrappers is shown in a schematic drawing. The storage tank with a mixing element, the pumps in the primary and secondary circuits, the visualization domain [10] and on the right hand side the heat exchanger can be seen.

Four cylindrical electrical resistance heating elements are mounted around an aluminum tube (figure 1, no. 8). The heating section has one meter length and an internal diameter of 23 mm. In the heat exchanger temperature profiles are measured at the inlet and outlet and in three further cross sections in the intermediate heating region. Their positions are shown in figure 2. Measurements

and data acquisition of surface temperatures and fluid temperatures, mass flow, density and pressure at the inlet and outlet are performed.

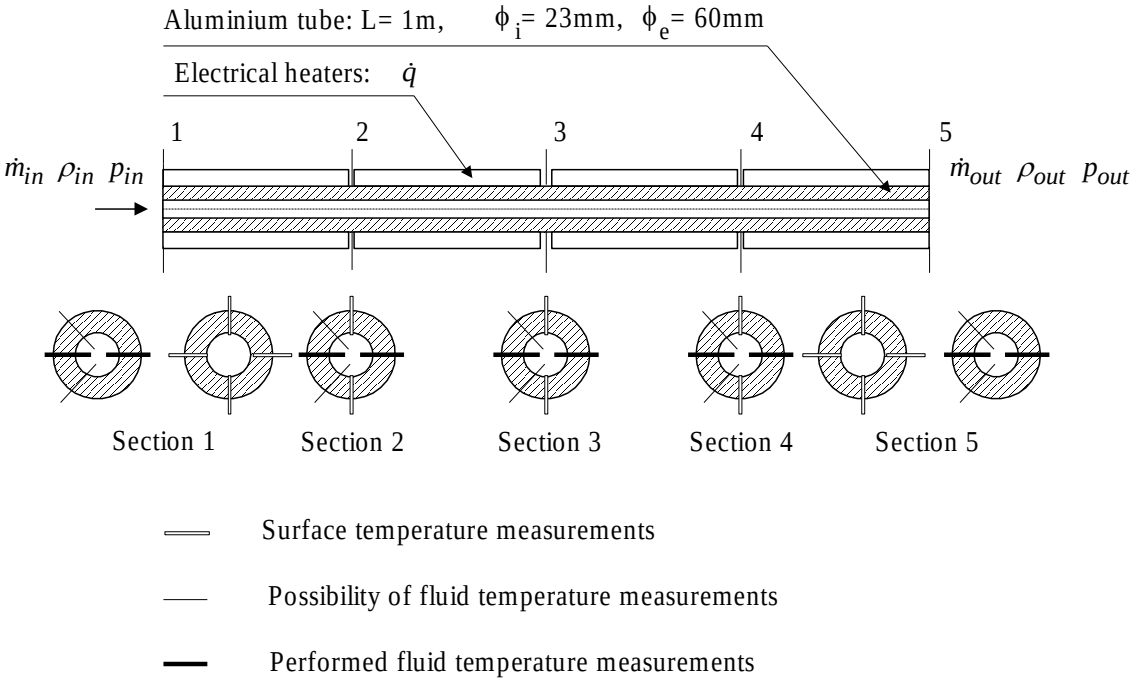


Figure 2: The cylindrical heat exchanger is equipped with four electrical heating elements, which define a constant-heat-flux-density boundary condition. Between the heating elements the probes can be continuously driven into the fluid to measure temperature profiles in cross sections perpendicular to the tube wall. In the cross sections at the inlet and outlet (section 1 and section 5) more possibilities exist to perform measurements. These are shown in two cross sections each. In this figure possible positioning of probes and the actually realized are clearly distinguished.

## 4. MEASUREMENT TECHNIQUES

In the refrigeration circuit the evaporation temperature is –13°C, the frequency of the scraper elements is 17.2 Hz and the angular frequency of the mixing device in the storage tank 23.5 Hz. In chapter 5.1 the mass flow, the inlet temperature and the heat flux are presented together with other parameters.

In the heat exchanger probes were mounted to the surface to measure the temperature on the inner surface of the tube. Further temperature probes - Pt-100 with a sensor length of 1.6 mm - permit local temperature measurements in the fluid. They are positioned in the tube perpendicularly to the wall. In each cross section two probes opposite of each other are operated. A first probe is positioned at the wall and is then moved to thirteen successive positions until it reaches the opposite side of the tube. At each position it is kept at rest for one minute to perform temperature measurements of the stationary flow. Mean values of at least five measurements are calculated. This operation is repeated by a second probe from the other side of the tube. Pulling one probe through a cross section leads to less disturbances than adjusting a large number of fixed probes. It is experienced

that good results are obtained in the opposite half of the pipe section. If the probe is pulled towards the wall on the side where the sensor enters the tube, a heat flux from the heating elements directly into the probes is observed. This phenomenon disturbes the measurements and causes too high temperature results. Therefore, only temperatures measured in the more distant half of the cross sections have been evaluated. The temperature measurements close to the heating elements at the wall have to be improved.
To determine heat transfer coefficients, respectively Nusselt numbers, signals of the fixed surface temperature sensors were processed.

To check the consistency of measured data, at the inlet and outlet of the heat exchanger two different probes - with an accuracy of $\pm$ 0.023 °C - were mounted. The detecting area of these probes has a length of 30 mm. Therefore, they directly measure the mean temperatures in the cross sections.

## 5. TEMPERATURE PROFILES

### 5.1 Parameters

The presented theory (and numerical program) of chapter 2 is applied. Because it is only valid for small heating rates - which do not produce too high nonlinearities – the heating power is chosen to be only 1018 W. A disadvantage of this small heat input is that the temperature differences in the fluid are small, and that the limits of reasonable accuracies of the measuring systems are approached.

The experiments and numerical calculations were performed with the following parameters:

| | | |
|---|---|---|
| Inner diameter of heat exchanging tube: | $d$ = 23 mm | |
| Length: | $l$ = 1.00 m | |
| Mass flow: | $\dot{m}$ = 0.355 kg/s | |
| Total electrical heating power: | $P$ = 1018 W | |
| Heat flux density: | $\dot{q}$ = 14100 W/m$^2$ | |
| Temperature of ice slurry at the inlet: | $\vartheta$ = -4.939 °C | |
| Ice fraction: | $c_I$ = 16 % | Ref. [5] |
| Density: | $\rho$ = 975.2 kg/m$^3$ | Ref. [5] |
| Specific heat: | $c_p$ = 40 300 J/(kg K) | Ref. [5] |
| Dynamic viscosity: | $\mu$ = 0.01 Pas | Ref. [11] |
| Critical shear stress: | $\tau_0$ = 5 Pa | Ref. [11] |
| Thermal conductivity: | varied (see in the remainder) | Refs. [12], [13] |

Table 1: Parameters defined for an experimental and numerical testing example of the heat transfer to an ice slurry in a tube with a constant-heat-flux-density boundary condition.

The density, the specific heat, the dynamic viscosity and the critical shear stress are based on experimental data. For the thermal conductivity at present no reliable measurements are available. In our investigations the quantities calculated with the model of Jeffrey have been applied. The references, where the numerical values of these properties can be found, are given in table 1.

### 5.2 Laminar Flow

First numerical simulations have been performed with a thermal conductivity of [13]

$k$=0.7 W/(m K) (12)

and a heat flux density reduced by a factor ten compared with the value given in table 1. The temperature profile at the outlet is shown in figure 3. It is seen that a small boundary layer near the wall is heated up and that, because of the very low thermal conductivity, the heat does not have time to reach the center of the tube. The high rise in boundary layer temperature causes that the limit of application of the model in this domain is exceeded. The following rough estimation also confirms the result of a low heat diffusion velocity. The thermal penetration depth $s$ can be estimated by

$$s = \sqrt{a\Delta t} = \sqrt{a\frac{l}{< u^{(0)} >}}, \qquad a = \frac{k}{\rho < c_p >_r} \tag{13a,b}$$

The results with the parameters of table 1 are

$$a = \frac{0.7\frac{W}{m\ K}}{975.2\frac{kg}{m^3}\,40300\frac{J}{kgK}} = 1.78\cdot 10^{-8}\,\frac{m^2}{s}, \qquad s = \sqrt{1.78\cdot 10^{-8}\,\frac{m^2}{s}\cdot\frac{1m}{0.876\frac{m}{s}}} = 0.14mm\,. \tag{14a,b}$$

The penetration depth is very small. From this result it is concluded that heat exchangers for ice slurries with laminar flows will not work very efficiently. This result corresponds with the reported low values of heat transfer coefficients measured with laminar flow conditions [13]. Better heat transfer is obtained when turbulent flow occurs (see chapter 5.3).

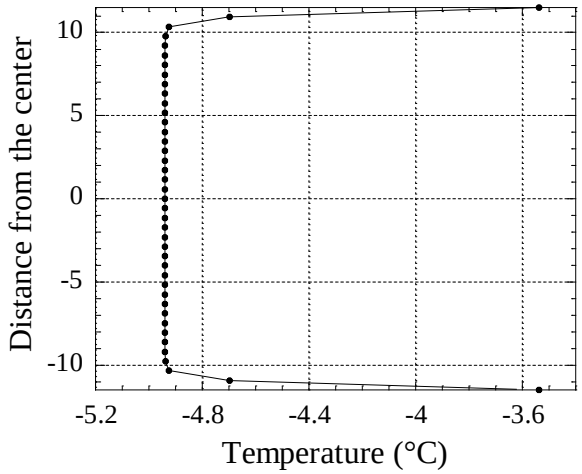


Figure 3: Profile of laminar ice slurry flow at the outlet of the heat exchanger. The heat has only little time to diffuse toward the center, before it is swept out of the tube by forced convection.

### 5.3 Turbulent Flow

The most simple approach to describe turbulent momentum and heat exchange is based on the eddy viscosity idea, respectively the turbulent Prandtl number concept. For a turbulent flow description equation (10) is generalized to [14]

$$\frac{\partial \overline{T}^{(1)}}{\partial x} - \frac{1}{\overline{u}^{(0)}} \left\{ a^{(0)} \left( \frac{1}{r} \frac{\partial \overline{T}^{(1)}}{\partial r} + \frac{\partial^2 \overline{T}^{(1)}}{\partial r^2} \right) + \frac{1}{r} \overline{T'v'} + \frac{\partial}{\partial r} \overline{T'v'} \right\} = 0 , \tag{15}$$

where the time-averaged and first-order temperature $\overline{T}^{(1)}$ occurs. Introducing an eddy-viscosity concept the gradient turbulence model is

$$\overline{T'v'} = -\varepsilon_h \frac{\partial \overline{T}}{\partial r} . \tag{16}$$

The problems related to gradient-type turbulence models have been discussed by several authors, for example by Egolf proposing a non-local Ansatz, named the difference-quotient turbulence model (DQTM) [15]. Nevertheless, introducing equation (16) into (15) it follows

$$\frac{\partial \overline{T}^{(1)}}{\partial x} - \frac{1}{\overline{u}^{(0)}} \left( a^{(0)} + \varepsilon_h \right) \left( \frac{1}{r} \frac{\partial \overline{T}^{(1)}}{\partial r} + \frac{\partial^2 \overline{T}^{(1)}}{\partial r^2} \right) = 0 . \tag{17}$$

It is known that in turbulent flows with an increasing Reynolds number the velocity profiles become more bulbous. In a laminar Bingham flow, caused by the plug, the profile is already very bulbous. For that reason in a first approximation in equation (17) the profile $u^{(0)}$ is applied.

In figure 4 for each of the five sections (also shown in figure 2) numerically calculated velocity profiles are compared with measured counterparts. The agreement is good. It is found that an eddy viscosity of $\varepsilon_h$=6.4 mm$^2$/s substituted into the numerical program leads to the best agreement. Multiplying by the density and specific heat a „turbulent conductivity“ of 250 W/m K is calculated, which is 360 times higher than the effective thermal conductivity, which is predicted by the model of Jeffrey: $k$=0.7 W/(m K) [13].

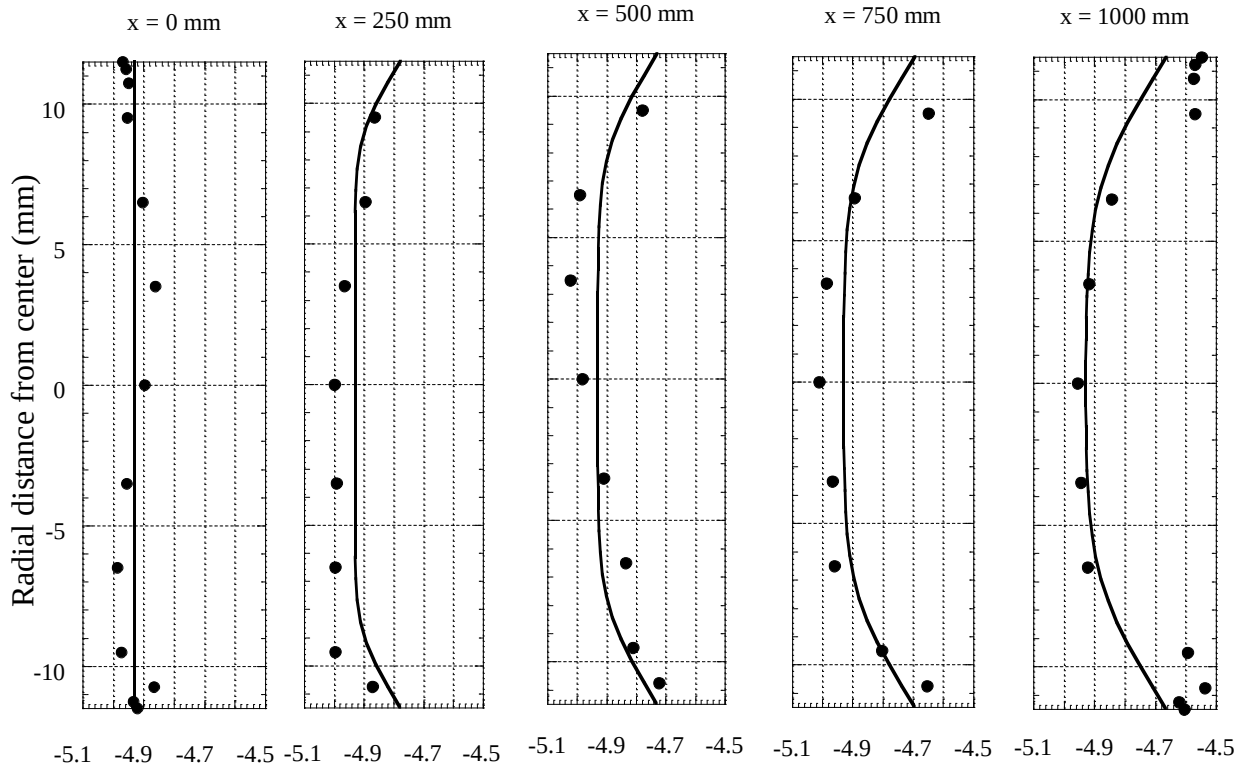

Temperature (°C)

Figure 4: Numerically calculated temperature profiles (curves) are compared with measured profiles (black dots). The cross sections one (x = 0 mm) to five (x = 1000 mm) correspond with the five sections shown in figure 2. The flow direction is from the left to the right. At the inlet of the heat exchanger a constant temperature boundary condition is realized. The surface temperatures of sections two to four are found to be at higher values and are not shown in these figures.
The next figure shows the calculated enthalpy flux density at the outlet of the heat exchanger as a function of the radial distance from the centerline of the tube. The maximal transport capacity is located at a radius of 9.3 mm and at the center there occurs practically no heat transport. This example demonstrates how important it is to understand the transport phenomena to correctly design and calculate heat exchangers.

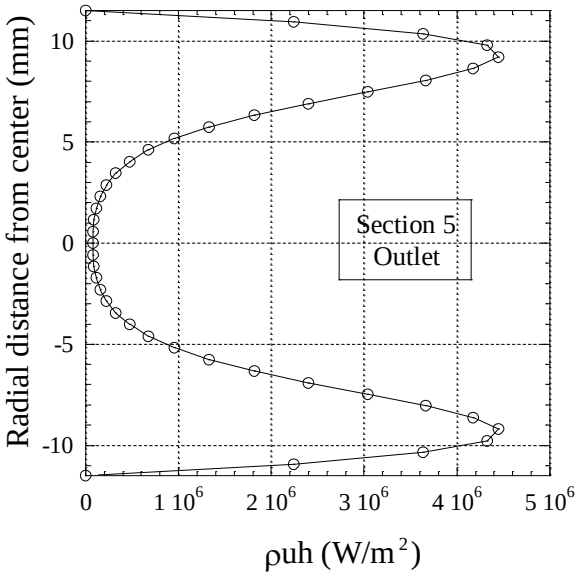


Figure 5: The enthalpy flux density in the outlet is shown. The integral of this curve over the cross section in cylindrical coordinates is 1017.7 W, which after rounding is identical to the electrical power of the heating elements P=1018 W (compare with value in table 1). Even in low-Reynolds number turbulence in 1.2 s the heat is not transferred to the center line of the tube. The time difference 1.2 seconds is the mean time, which an ice particle needs to pass the heat exchanger tube.

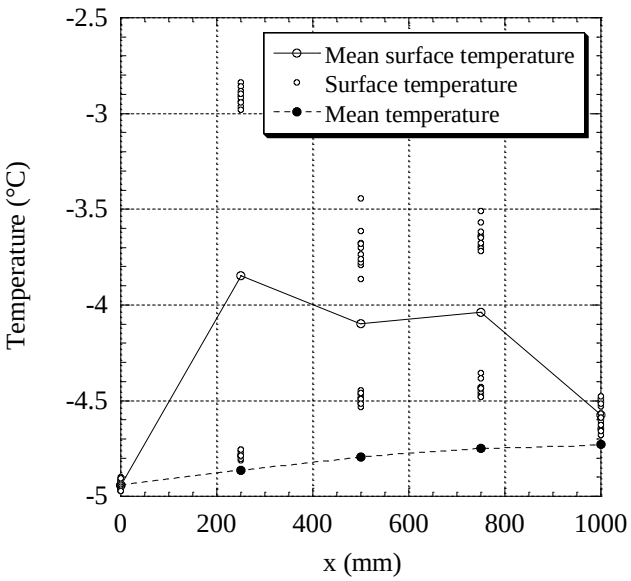

Figure 6: Surface temperatures at different positions (e.g. top and bottom of pipe) determined by experiments and mean temperatures determined by experiments and numerical calculations (figure 4). The mean temperature downstream is not a linear function of the downstream coordinate, which can be seen by an amplification of the figure. This occurs because of a correlation of enthalpy and velocity as explained in Ref. [9]. The surface temperature measurements show large scattering and must be further improved.

It is clear that in a heat exchanger with a constant-heat-flux-density boundary condition the enthalpy flux density $<\rho u h>_r$ has to increase linearly as a function of the downstream coordinate x. This is even correct when physical properties alter as a function of temperature. The same argument does not necessarly apply for the mean temperature (see Ref. [9])

$$< T >_r = \frac{1}{A_P} 2\pi \int_0^R T(r) r dr \qquad A_P = \pi R^2 . \tag{18a,b}$$

The mean temperature in each cross section is shown in figure 6. In this figure also the surface temperatures measured with the surface temperature probes and the probes to measure profiles - by positioning them at the wall - are shown. In the inlet the surface temperature is equal to the constant fluid temperature. Further downstream the surface temperatures are much higher than the fluid temperatures. On the other hand in figure 4 the profiles fulfill energy conservation requirements. From this it is concluded that there must be a boundary layer with a very low enthalpy content. Therefore, a boundary layer is expected to occur, which is very thin. Because in this layer the flow is laminar, the low thermal conductivity leads to a very high temperature derivative perpendicular to the wall

$$\frac{\partial T}{\partial r} = \frac{\dot{q}}{k} = \frac{14100 \frac{W}{m^2}}{0.7 \frac{W}{mK}} \cong 20 \frac{K}{mm} . \tag{19}$$

In figure 6 it is shown that the temperature difference between the surface and the bulk of the fluid is approximately 1 K. With equation (19) a boundary layer thickness of 0.05 mm is estimated, which is of the size of an ice crystal. As it is seen from the following formula

$$\alpha(x) = \frac{\dot{q}(x)}{T_S(x) - < T >_r (x)}, \tag{20}$$

this boundary layer reduces the heat transfer coefficient, because it causes a larger temperature difference. – Numerous heat transfer coefficients have been calculated and are presented in the next chapter.

## 6. HEAT TRANSFER COEFFICIENTS

The evaluation of the heat transfer coefficients for laminar flow is shown in figure 7. To calculate the dimensionless numbers the physical properties reported in the references cited in table 1 were

applied. The small circular markers show results, which are related to different sections of the heat exchanger (figure 2). They are not specially distinguished in this presentation. The larger black markers show the mean values of each experimental series at a particular Reynolds number. The range of investigated Reynolds numbers is written on the figure. On the left, characterized by a large rectangular marker, the Nusselt number of water/ethanol - without any ice fraction - is shown. This value is Nu = 4.3. The Nusselt number is presented as a function of the Hedström number. This dimensionless number characterizes the ice fraction of the ice slurry. Toward higher Hedström numbers, respectively ice fractions, the Nusselt number continuously increases as expected by a simple physical explanation.

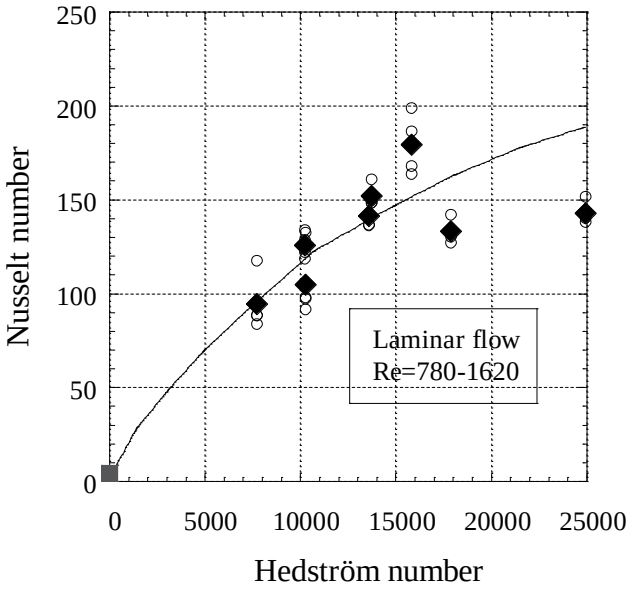


Figure 7: The Nusselt number as a function of the Hedström number, characterizing the Bingham effect, is shown for laminar flow. On the left, presented by a rectangular marker, the Nusselt number of water/ethanol without any ice fraction is shown.

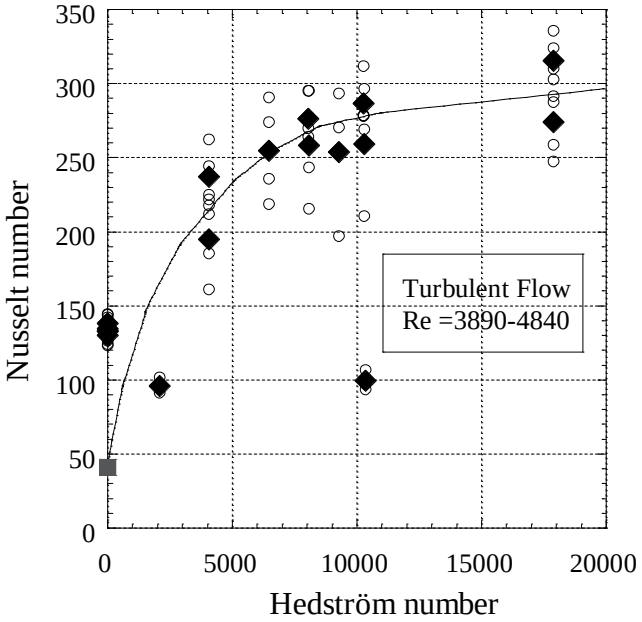

Figure 8: The Nusselt number as a function of the Hedström number is shown for turbulent flow. The heat transfer is higher in turbulent flow than in laminar flow. This corresponds with the physical idea that turbulent fluctuations lead to an additional heat transport.

The heat transfer coefficients of turbulent flow are higher than those determined for laminar flow. At an ice fraction zero (Hedström equal to zero) the theoretical Nusselt number of water/ethanol, calculated by the well-known formula of Gnielinski, is Nu = 41. Again the measured data converge toward the theoretical Nusselt number in the Newtonian limit of zero ice fraction.

The surface temperature measurements have to be improved taking more than one measuring method into consideration. Furthermore, experiments have to be repeated performing measurements at a larger number of positions per cross section and by collecting large data sets at each position in the cross section. Then by basic laws of statistics the accuracy of the temperature profiles even close to the surface of the tube, where higher fluctuations in the temperature data have been observed, can be improved.

## 8. CONCLUSIONS AND OUTLOOK

A fluiddynamic and thermodynamic model derived by a perturbation analysis has been taken to construct a new numerical program. With this program temperature profiles can be correctly calculated for laminar flows, but only very approximately for turbulent flows. For the latter case improvements are under consideration.

First measured temperature profiles of ice slurry flows are presented. The theoretical and the experimental profiles compare well. The thermal conductivity, the only relevant physical property that has not been measured yet, is taken from a model presented in the literature. Proposals to determine the thermal conductivity or the thermal eddy diffusivity, which is an empirical parameter, are presented in Ref. [6].

New measurements of the FIFE group on heat transfer coefficients are presented. A consistent picture is obtained. In the limit of zero ice fraction the measurements converge toward the well-known values. As expected the Nusselt numbers are higher for turbulent than for laminar flow.

Further experimental and numerical work is planned for higher heat transfer rates leading to high non-linearities.

## NOMENCLATURE

**Standard**

| | | |
|---|---|---|
| $A$ | area | ($m^2$) |
| $c_p$ | specific heat | (J/kg K) |
| $h$ | enthalpy density | (J/kg) |
| $k$ | thermal conductivity | (W/m K) |
| $\dot{m}$ | mass flow | (kg/s) |
| $p$ | pressure | (Pa) |
| $\dot{q}$ | heat flux density | ($W/m^2$) |

| | | |
|---|---|---|
| $r$ | radial co-ordinate | (m) |
| $r_1$ | radius of plug | (m) |
| $r_2$, $R$ | radius of pipe | (m) |
| $T$ | temperature | (°C) |
| $T_m$ | mean temperature of a cross section | (°C) |
| $T_s$ | surface temperature | (°C) |
| $u$ | velocity | (m/s) |
| $x$ | space co-ordinate downstream | (m) |

**Greek**

| | | |
|---|---|---|
| $\alpha$ | heat transfer coefficient (German notation) | (W/m$^2$ K) |
| $\chi$ | general variable | (-) |
| $\varepsilon_h$ | thermal eddy diffusivity | (m$^2$/s) |
| $\mu$ | dynamic viscosity | (Pas) |
| $\rho$ | density | (kg/m$^3$) |
| $\tau_0$ | critical shear stress | (Pa) |

**Dimensionless numbers**

| | |
|---|---|
| *He* | Hedström number |
| *Nu* | Nusselt number |
| *Pr* | Prandtl number |
| *Re* | Reynolds number |

## ACKNOWLEDGEMENTS

We thank Ph. Moser for engineering support. We are grateful to A. Cavin for many useful advices and G. Chollet for continuous technical assistance. The support of the FIFE work by *the "Projekt- und Studienfonds der Elektrizitätswirtschaft (PSEL)"*, the *"Kommission für Technologie und Innovation (KTI)"* and the *„Haute École Speciale – Suisse Occidentale (HES-SO)"* is gratefully acknowledged.

## REFERENCES

[1] Graetz, L., 1885, Ueber die Wärmeleitungsfähigkeit von Flüssigkeiten, *Annalen der Physik und Chemie* **7**, 337-357.

[2] Grigull, U., 1956, Wärmeübergang an nicht-Newtonsche Flüssigkeiten bei laminarer Rohrströmung, *Chemie-Ing.-Techn.* 28. Jahrgang **8/9**, 553-556.

[3] Wissler, E. H., Schechter, R. S., 1959, The Graetz-Nusselt Problem (with Extension ) for a Bingham Plastic. *Chem. Eng. Prog. Symposium* Series No. **29**, 55, 201-208.

[4] Thomas, D. G., 1960, Heat and Momentum Transport Characteristics of Non-Newtonian Aqueous Thorium Oxide Suspensions, *A. I. Ch. E. Journal* **6**, 4 631-639.

[5] Egolf, P. W., Frei, B., 1999, The Continuous-Properties Model for Melting and Freezing applied to Fine-Crystalline Ice Slurries. *Proceedings of the First IIR Workshop on Ice Slurries*, 25-40, Yverdon-les-Bains, 28-29 May.

[6] Egolf, P. W., Sari, O., Meili, F., Vuarnoz, D., Moser, Ph., 2000, *Thermodynamics of Moving and Melting Ice Slurries in Pipes*: *Theory, Numerical Simulations and Comparisons with Measurements*. EUREKA FIFE report No. 5, June.

[7] Egolf, P. W., Brühlmeier, J., Özvegyi, F., Abächerli, F., Renold, P., 1996, *Kältespeicherungseigenschaften von Flo-Ice®.* Forschungsbericht zuhanden der Stiftung zur Förderung des Zentralschweizerischen Technikums Luzern.

[8] Govier, G. W., Aziz, K., 1972, *The Flow of Mixtures in Pipes*. Van Nostrand Reinhold Publishing Company, New York.

[9] Egolf, P. W., Sari, O., Meili, F., Moser, Ph., Vuarnoz, D., 1999, Heat Transfer of Ice Slurries in Pipes. *Proceedings of the First IIR Workshop on Ice Slurries*, 106-123, Yverdon-les-Bains, 27-28 May.

[10] Sari, O., Vuarnoz, D., Meili, F., Egolf, P. W., 2000, Visualization of Ice Slurries and Ice Slurry Flows. *Proceedings of the Second IIR Workshop on Ice Slurries*, Paris, 25-26 May (accepted).

[11] Frei, B., Egolf, P. W., 2000, Viscometry Applied to the Bingham Substance Ice Slurry. *Proceedings of the Second IIR Workshop on Ice Slurries*, Paris, 25-26 May (accepted).

[12] Bel, O., 1996, Contribution à l'étude du comportement thermo-hydraulique d'un mélange diphasique dans une boucle frigorifique a stockage d'énergie, Ph D thesis, No. 96 ISAL 0088, L' Institute National des Sciences Appliquées de Lyon, France.

[13] Lakhdar, M. A .B., 1998, *Comportement thermohydraulique d'un fluide frigoporteur diphasique: le coulis de glace*, Ph D thesis, L' Institut National des Sciences Appliquées de Lyon, France, April.

[14] Cebeci, T., Bradshaw, P., 1984, *Physical and Computational Aspects of Convective Heat Transfer*. Springer-Verlag, New York.

[15] Egolf, P. W., Difference-quotient turbulence model: a generalization of Prandtl's mixing-length theory, *Phys. Rev. E* **49**, No. 2, 1260-1268.